Quantification of Lung Stiffness Using Magnetic Resonance Elastography (MRE): Clinical Validation for Smokers

Sabine F Bensamoun, Kiaran P Mcgee, Mashhour Chakouch, Philippe Pouletaut, Fabrice Charleux

Quantification of Lung Stiffness Using Magnetic Resonance Elastography (MRE): Clinical Validation for Smokers

Sabine F. Bensamoun*, Kiaran P. McGee, Mashhour Chakouch, Philippe Pouletaut, Fabrice Charleux

***Abstract*— *Objective:* Tobacco-related pathologies are the most preventable diseases. The purpose is to provide personalized cartography of smoker lung stiffness using non-irradiating imaging modalities, MRI and MRE (magnetic resonance imaging/elastography). *Methods:* Thirty-four smokers were divided into five groups distributed with a range of pack-years (PY) of 10. All patients underwent three imaging tests (CT: computed tomography, MRI, MRE) to make possible measurements of lung density, with two modalities (CT, MR), and stiffness. CT lung density was measured using the Hounsfield number. MR density was obtained from a fast gradient echo sequence and validated with an *in vitro* 3D abdominal phantom. The MRE test was performed with a motion-encoding gradient (Z direction), a spin-echo echo-planar sequence and four offsets. A pneumatic driver (frequency: 50 Hz) was placed on the right lung and four axial phase images were recorded. Post-processing was then performed to record a personalized stiffness cartography. *Results:* CT density significantly increased in relation to PY, showing denser tissue for the heavy smokers. As MR density acquisition is less accurate than CT, a slight increase in lung density was obtained. MRE tests revealed a significant increase in stiffness with pack-year. Patient-specific lung stiffness showed inhomogeneous distribution of values. *Conclusion:* MRE could provide a personalized cartography of stiffness for regular uptake of the lung's mechanical behavior in smokers. The stiffness could become a biomarker for preventing future lung disease. *Significance:* MRE test could be an alternative to CT test for the follow-up of smokers.**

***Index Terms*— Abdominal phantom, Computed tomography, Magnetic resonance elastography, Personalized stiffness, Smoker.**

I. Introduction

In 2040, the European commission aims to achieve a tobacco-free Europe. Tobacco smoking causes over 8 million deaths worldwide annually [1] and is responsible for 80 % of lung cancer in Europe [2], [3], [4]. Smoking can be the result of several factors such as stress, addictions (alcohol, …), and social conditions [5]. Depending on tobacco consumption, which is estimated in pack-years (PY), the smoking profile can be normal (i.e. PY of less than 20) or severe (i.e. PY of more than 20) leading to health risk factors [6].

To prevent and reduce these risks, governmental actions have been proposed [7]. Gredner's study [4] showed that implementing tobacco control policies could have a significant impact in Europe with regard to reducing the incidence of lung cancer. Moreover, other nicotine delivery devices [8] encouraged both the decrease in tobacco dependence and stopping smoking [9]. Vaping has been promoted since electronic cigarettes started to be commercialized in 2010 [10]. The substances inhaled from electronic cigarettes are less toxic than the 5000 components of cigarettes, composed of at least 50 carcinogens [11]. However, no quantitative scientific data have shown that vaping is less harmful, and in 2019 the World Health Organization (WHO) advocated for regulation of its use [12].

Another way to evaluate health risks is to monitor the functionality of smokers' lung tissue [13]. A clinical test, known as the pulmonary function test (PFT) or spirometry test, is thus available. It is mainly carried out by the pulmonologist and makes it possible to evaluate the maximum volume the patient can exhale in one second (forced expiratory volume in one second (FEV1)) and forced vital capacity (FVC). Based on these measurements, a classification related to the GOLD (Global Initiative for Chronic Obstructive Lung Disease) clinical scale can graduate the level of lung fibrosis from light (Gold I: FEV1 > 0.8) to severe (Gold IV: FEV1 < 0.3) with FEV1 / FVC < 0.7 [14].

To complete the PFT test, computed tomography (CT) is currently performed to analyze the structural properties of smokers' lung tissue. Tobacco smoking effectively induces abnormal responses in lung tissue at different scales [15], resulting in specific tobacco pathologies such as chronic obstructive pulmonary disease (COPD), as well as chronic bronchitis and emphysema, interstitial lung disease and fibrosis [16]. Each disease has a morphological signature [17] which can be followed over time. However, the modality of CT imaging does not provide quantitative data for quantifying the mechanism of the lungs. Moreover, CT uses X-rays, limiting regular follow-up of smokers' lungs based on the ALARA principle [18], [19].

It is worth noting that a novel approach was presented by Hasse et al. [20] to show the feasibility of performing low dose CT. These acquisitions made possible better accuracy of the distribution of stiffness inside the lung, which was estimated from a biomechanical constitutive model using four dimensional CT images [21].

This work was co-founded by the European Union through the European Regional Development Fund (FEDER) within the framework of the Contrat de Plan Etat-Région (CPER) 2021-2027 for the Hauts-de-France region.

*S.F. Bensamoun (sabine.bensamoun@utc.fr), P. Pouletaut (philippe.pouletaut@utc.fr) and Mashhour Chakouch (mashhour.chakouch@utc.fr) are with Université de technologie de Compiègne, CNRS, Biomechanics and Bioengineering, Compiègne, France.

F. Charleux (fabrice.charleux@acrim.fr) is with ACRIM-Polyclinique Saint-Côme, Medical Radiology, Compiègne, France.

K.P. McGee (mcgee.kiaran@mayo.edu) is with Mayo Clinic & Foundation, Department of Radiology, Rochester, Minnesota, USA.

Cartography of lung stiffness can also be obtained with other imaging modalities which have the advantage of not using radiation. Elastography modalities, based on shear wave propagation [22], using ultrasound or magnetic resonance imaging, have been used to characterize the mechanical changes in lung tissue. Shear wave elastography (SWE) was thus applied to interstitial lung disease (ILD) and changes in the mechanical properties were revealed through higher velocities [23], [24] and an increase in stiffness [25] in ILD lung tissue. Moreover, SWE was used to characterize stiffness in the respiratory muscles (diaphragm, intercostal muscle) in chronic obstructive pulmonary disease (COPD) patients and the data were correlated with the respiratory clinical score using the spirometry technique [26].

In addition to ultrasound elastography, magnetic resonance elastography (MRE) was also applied to various soft tissues [27], [28]. The Covid pandemic enhanced the development of the non-invasive MRE imaging technique for the functional characterization of lung tissue [29]. While the main composition of the lung is air, the feasibility of MRE for measuring lung stiffness [30] as well as MRE's sensitivity for assessing changes in stiffness as a function of age [31] and disease [32] have been demonstrated.

Characterization of smokers' lungs is of importance because tobacco-related pathologies are the most preventable diseases. Early detection and regular monitoring methods are essential. The purpose of this study is to provide personalized cartography of stiffness in smokers' lungs, using a non-irradiating imaging modality, which would become a biomarker for preventing future lung disease and trigger awareness of the patient regarding the state of their lung function through a visual color scale.

II. Methods

A. Participants

Thirty-four current smokers (7 men, 27 women) were recruited at the radiology department, named ACRIM, located at the Polyclinic Saint Côme (Compiègne, France). All patients have approximately the same body mass index (mean BMI 24.0 ± 4.2 $kg.m^{-2}$) and age (mean age 50.5 ± 9.7 years) (Table 1). They were referred for a lung CT scan, without injection of contrast product, to analyze moderate tobacco symptoms (such as cough, bronchitis) or for a simple lung checkup related to the level of tobacco consumption. Exclusion criteria were the contraindications for MRI (such as pregnancy, claustrophobia, pacemakers), people under the age of 18 years, without emphysema and lung fibrosis such as chronic obstructive pulmonary disease (COPD).

In accordance with the United States Preventive Services Task Force (USPSTF), the current smokers were divided into five groups in relation to their smoking pack-years (PY), with a range of 10 PY. Pack-years are calculated as smoking duration in years multiplied by number of cigarettes per day, and divided by 20 (number of cigarettes in a pack). This information was provided by the patient during the interview.

This study was approved by the Institutional Review Board of ILE DE FRANCE III (#2020-A01496-33). All subjects had the experimental protocol explained, a reflection period, and then gave their informed written consent prior to admission into the study.

B. Computed Tomography (CT) Scan

Current smokers had a single CT scan test at total lung capacity. Lung CT images were acquired with a multi-row detector system (Revolution Maxima, General Electric HealthCare, Chicago, USA). Patients were examined during a single breath-hold and the following parameters were applied for the thoracic CT acquisition: field of view (FOV): 37 cm; matrix: 512 x 512; pixel size: 0.72 mm; slice thickness: 0.625 mm and 100 to 140 kV depending on the patient's weight. A senior radiologist visually analyzed the texture and structural properties (bronchial thickness, absence of emphysema, etc.). In addition, when the intermediate trunk was clover-shaped in appearance, showing the origin point of tertiary bronchi, the slice level was identified (Fig. 1 a-b) for future MRE assessment (Fig. 1 c) of the same lung region. CT density was calculated by converting the measured Hounsfield number into density units [33].

TABLE I
CHARACTERISTICS OF THE COHORT OF SMOKERS. RESULTS ARE PROVIDED AS MEDIANE (INTERQUARTILE RANGE). SYMBOLS * AND ** INDICATE STATISTICAL SIGNIFICANCE ($p < 0.05$) AND ($p < 0.01$) FROM TWO-SAMPLE MANN-WHITNEY'S TEST (U-TEST) BETWEEN TWO ADJACENT RANGES OF PY.

PY range	PY < 10	10 ≤ PY < 20	20 ≤ PY < 30	30 ≤ PY < 40	PY ≥ 40
Number of smokers	4	9	9	8	4
Number of women	3	6	6	8	3
Age (year)	48.6 (12.4)	49.8 (22.7)	43.7 (8.9)	55.6 (13.3)*	55.9 (3.0)
BMI ($kg.m^{-2}$)	28.9 (6.7)	23.0 (4.1)	21.8 (3.3)	24.1 (3.9)	25.9 (3.5)
Delay between MRE & CT tests (day)	15 (10)	35 (18)	24 (16)	29 (43)	45 (18)
CT lung density ($kg.m^{-3}$)	162 (23)	137 (15)	181 (48)*	151 (42)	170 (20)
MR lung density ($kg.m^{-3}$)	176 (18)	136 (29)	164 (77)	164 (35)	187 (39)
Lung stiffness (kPa)	1.38 (0.32)	1.17 (0.27)	1.80 (0.47)**	1.93 (0.35)	1.62 (0.67)

BMI = body mass index; CT = computerized tomography; MRE = magnetic resonance elastography; PY = pack-years.

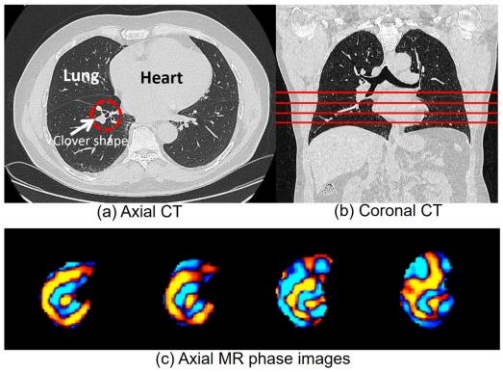

Fig. 1. a. Localization of the clover shape in axial CT acquisition. b. positioning of the four axial slices (red line) inside the clover shape in the CT coronal view. c. axial MR phase image acquisitions.

C. Lung Density

The lungs are mainly composed of air, so to provide a personalized cartography of stiffness, it was necessary to acquire a cartography of each patient's lung density.

This mapping was obtained from MRI (1.5 T, Signa Artist, General Electric HealthCare, Chicago, USA) acquisition performed at breath-hold (22 s) at total lung capacity. A respiratory belt is attached around the abdomen to monitor the level of lung capacity providing a respiratory feedback. Then, 4 axial slices were recorded at the same thoracic level where the CT clover-shape was localized, with a fast gradient echo (GRE) sequence [34] and a TR of 15 ms, from which the initial signal of the lung was estimated. The MRI acquisition was performed with the following parameters: FOV: 48 cm; pixel size: 3.75 mm; matrix: 64 x 64; slice thickness: 15 mm; and flip angle: 10°. Before running the MR density sequence, a gadolinium-doped water phantom was placed on the sternum for calibration [35], and the density values were validated with the CT density measurements.

The lung density map was computed in three steps:

1) Image acquisition of MR signal at 8 echo times tj (TE1 = 1.828 ms and then TE2 = 1.028 ms repeated four times): Ij = I0 exp (- tj / T2*) for determining the initial signal I0 and relaxation time T2*;

2) Calibration acquisition with gadolinium-doped water phantom for determining a correction factor (CF) from MR acquisition at two repetition times (TR):

CF = (mean phantom signal at TR = 6 s) / (mean phantom signal at TR = 10 ms) (1)

3) Calculation of the lung density map (ρ):

$$\rho = I0 / (CF \times Iph) \quad (2)$$

where Iph is the mean signal of the gadolinium-doped water phantom, CF the correction factor, and I0 the mean signal of the lung at an echo time of zero [36].

In these steps, the correction factor measurement is needed because it depends on MR machine [36]. The value of the correction factor with the present MR machine was 2.25.

D. Magnetic Resonance Elastography (MRE)

MRE tests were performed at the same slice level as MRI density acquisitions, using a spin-echo echo-planar imaging (SE-EPI) sequence on a 1.5 T General Electric Signa Artist machine to obtain 4 axial phase images (Fig. 1 c) of the lung. MRE measurements were made at total lung capacity, with a 22 s breath-hold for the scan time. This sequence was designed for a reduction of overall scan time with an increase in T1-dependent signal recovery [30], [37]. It included fat saturation signal, an echo train length of 8, a time echo of 12.8 ms, a two unipolar motion encoding gradient (MEG) lobes (duration 2 ms), and a minimum achievable TR of 320 ms. The higher TR compared to a regular SE sequence (200 ms) provided a higher MR signal related to the T1 value (about 1300 ms) of the lung parenchyma [37].

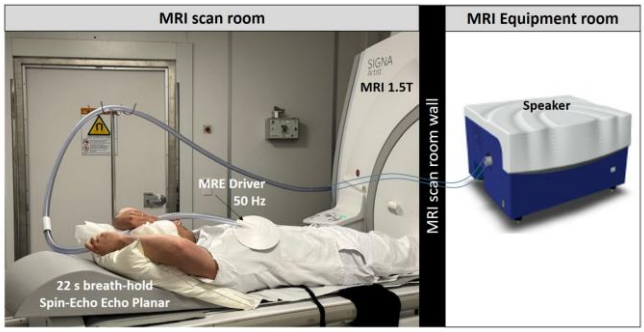

Fig. 2. Magnetic resonance elastography (MRE) set-up.

A respiratory belt is attached around the abdomen to monitor the level of lung capacity providing a respiratory feedback. Then, a round pneumatic driver (Resoundant, Mayo Clinic Foundation, Rochester, MN, USA), currently used for MRE liver tests [38], was placed on the right lung to avoid the motion artifact of the heart (Fig. 2). This driver was connected to a plastic tube where air pressure was induced at a frequency of 50 Hz using an acoustic speaker system.

The MRE pulse sequence, including a motion-encoding gradient which oscillated in the Z direction, was used to image the displacement of the shear waves. The phase images were recorded with the following parameters: FOV: 48 cm; TR: 250 ms; slice thickness: 15 mm; number of axial slices: 4; pixel size: 3.75 mm; matrix: 128 x 128; 4 phase offsets.

To measure lung stiffness, different steps were performed by two medical imaging engineers with more than ten years of experience in the MRE field. Firstly, a region of interest was drawn to select only the right lung to avoid the motion of the heart, and secondly the apparent lung stiffness was calculated from the phase images using a multi-model direct inversion (MMDI) [39]. This inversion method used current mechanical assumptions (linear, elastic, isotropic, homogeneous and incompressible) on lung tissue material. The specific post processing method included phase unwrapping based on minimum discontinuity algorithm, four directional spatial Butterworth filter from 4 to 40 waves / FOV, to limit the noise and the interferences, and Romano smoothing filter with a circular 11 pixels diameter processing kernel [39].

Then, the personalized cartography of stiffness was obtained from the correction made with the cartography of density. In addition, the repeatability of the stiffness measurement was evaluated for 10 patients.

E. *Abdominal Phantom*

In addition to the *in vivo* analysis, an *in vitro* study was performed on a 3D abdominal phantom (CIRS, model 057A) to validate the *in vivo* process (analysis method, and imaging modalities: CT vs MRI acquisition) for the *in vivo* density measurements. This phantom was chosen as it contains the same surrounding tissues (such as intercostal muscle, ribs, fat) and the same internal organs (liver, spine) as those present during the *in vivo* acquisitions. CT and MRI acquisitions were performed with the same pixel size and the same thickness as in *in vivo* tests (Fig. 3) for each modality. In addition, the gadolinium-doped water phantom was also placed on top of the CIRS phantom (Fig. 3 a). A circular region of interest (ROI) (diameter 52.5 mm) was manually placed inside the lung area to measure the CT density [33] which was compared to CIRS density value. After that, the MR density calculated inside the same circular ROI (Fig. 3 b) was compared to the CIRS and CT densities values.

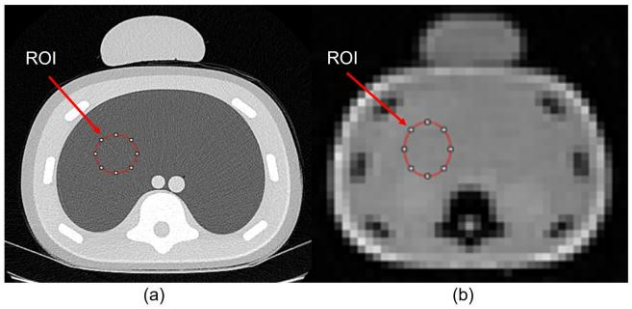

Fig. 3. CIRS abdominal phantom. a. CT axial acquisition. b. MR axial acquisition. A circular region of interest (ROI) of 52.5 mm diameter was placed in the right lung.

F. *Statistical Analysis*

All the statistical analyses were performed with R software [40]. Non-parametric two-sample Mann-Whitney U-tests were used to compare the following parameters: 1) lung density between each group of smokers (using CT or MR tests), 2) lung density in the CIRS phantom between CT and MR tests, and 3) lung stiffness between each group of smokers for the MRE test. Distributions of CT density, MR density and lung stiffness were found to consistently follow normal distributions using Shapiro–Wilk test. Thus, a correlation test with Pearson's correlation coefficient was realized to compare the CT density values with the MR density and the lung stiffness data. The level of significance was set at $p < 0.05$.

The intra-class correlation coefficient (ICC) was used to assess the agreement 1) between CT and MR modalities for lung density, 2) between two successive measurements of lung stiffness, and 3) between the two engineers who obtained the MRE lung stiffness. Agreement was classified as poor (ICC = 0.00-0.20), fair to good (ICC = 0.40-0.75) or excellent (ICC > 0.75) [41].

III. RESULTS

A. *Lung and Phantom Densities*

The density values were obtained with multimodality (CT, MRI) imaging techniques performed *in vivo* (smoker lung tissue) and *in vitro* (CIRS Phantom). CT density (ρ_{CT}) showed a significant ($p = 0.024$) increase in the median value (interquartile range (IQR)) in relation to the pack-year ($\rho_{CT\_10\leq PY<20}$ = 137 (15) kg.m^{-3} vs $\rho_{CT\_20\leq PY<30}$ = 181 (48) kg.m^{-3}) (Table 1, Fig. 4, Fig. 5). This result indicates the presence of denser tissue for the heavy smokers (PY ≥ 20). Moreover, important inter-individual variation (range from 119 to 180 kg.m^{-3}) was observed for both groups, revealing patient-specific physiological behavior.

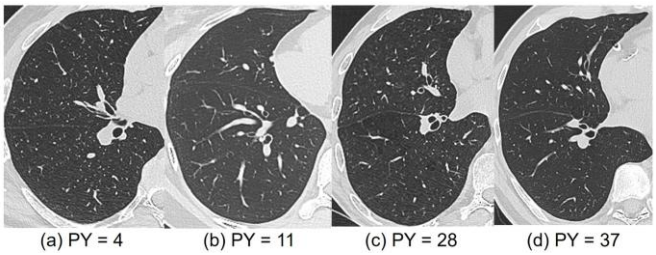

Fig. 4. CT axial acquisitions of 4 smokers with different pack-year (PY) values. a. PY = 4. b. PY = 11. c. PY = 28. d. PY = 37.

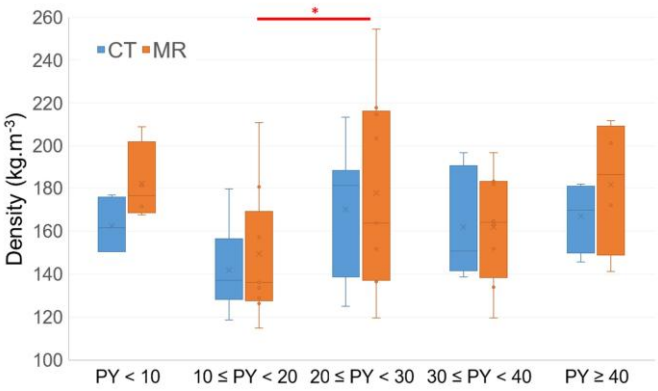

Fig. 5. Box-plots of the CT and MR lung density values for five groups of smokers according to different ranges of pack-year (PY). Symbol * indicates statistical significance ($p < 0.05$) from two-sample Mann-Whitney's test.

Concerning the MR density values (ρ_{MR}), a non-significant increase was obtained for the heavy smokers (PY ≥ 20) (Table 1, Fig. 6). This result follows the same trend as the CT density. The intra-class correlation coefficient and 95 % limits-of-agreement are evidence of good agreement (ICC = 0.75 [0.451 - 0.868]) between both imaging modalities (CT vs MR). It should be noted that the non-significant variation obtained for the MR densities between both smoker groups may be explained by the different characteristics of the modalities between CT and MR. The CT density measurement was realized over 100 CT slices compared to only 4 MR acquisitions. Moreover, the density result is dependent on slice thickness (MR: 15 mm vs CT: 0.624 mm) and pixel size (MR: 3.75 mm vs CT: 0.72 mm) which are better with the CT modality.

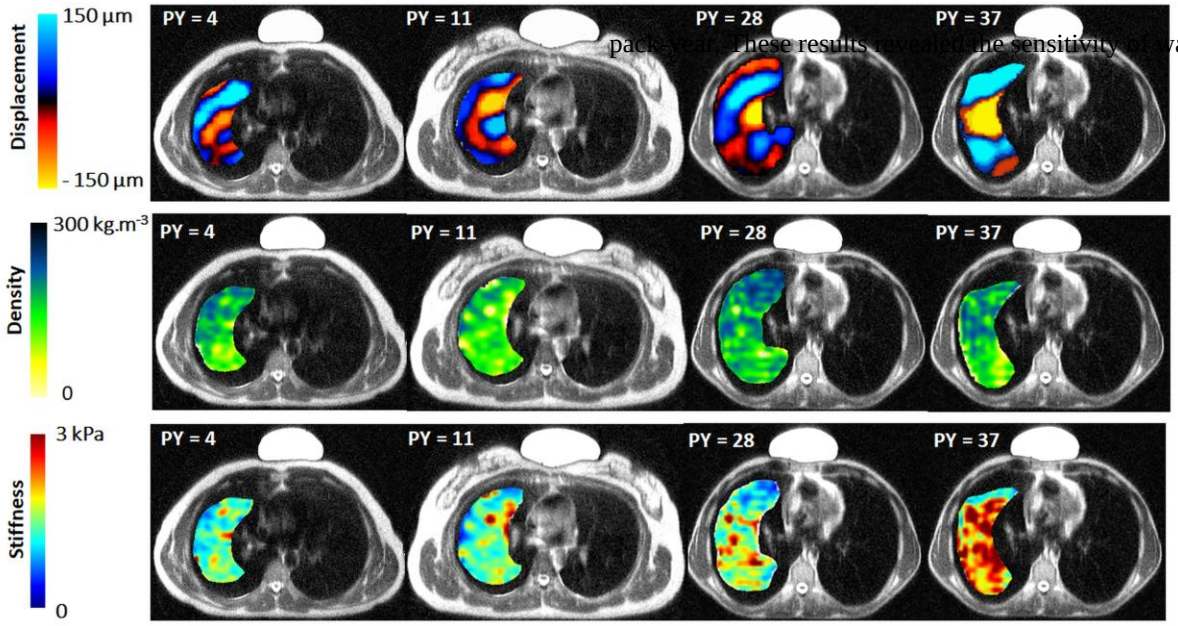

Fig. 6. MR axial images for four smokers with different pack-years (PY) and overlaid cartographies: displacement (top line), density (middle line) and stiffness (bottom line).smokers (pack-years (PY) < 20 and PY ≥ 20).

The correlation plot between CT density and MR density (Fig. 7) showed statistically significant correlation with Pearson's coefficient (r = 0.7421, p < 0.001).

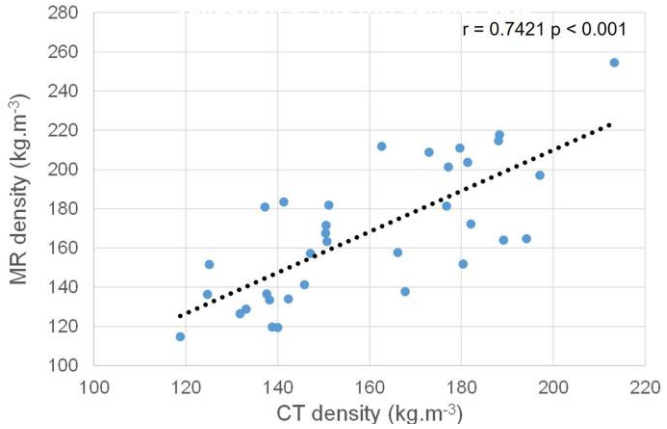

Fig. 7. Correlation plot between the CT and MR lung density values. The statistical test used is the correlation test with Pearson's coefficient *r*.

In parallel to *in vivo* measurement, density results were determined on the abdominal CIRS phantom. CT and MR densities were in the same range (mean (standard deviation) values in ROI: ρ_{MR} = 499 ± 79 kg.m^{-3} vs ρ_{MR} = 526 ± 19 kg.m^{-3}) and in accordance with the referent lung value (530 kg.m^{-3}) provided by the constructor (CIRS). In addition, this result made it possible to validate the correction factor (CF) value which was used to measure MR density. This result validated the processing method used for the *in vivo* lung density measurements.

B. Smoker Lung Stiffness

The phase images (Fig. 6), showing the displacement of the shear waves, indicated an increase in wave length in relation to propagation to the lung media. As a result, the stiffness (S) values also significantly (p = 0.0041) increased in relation to pack-year (median (IQR) values: $S_{10\leq PY<20}$ = 1.17 (0.27) kPa vs $S_{20\leq PY<30}$ = 1.80 (0.47) kPa) between both groups of smokers (Table 1, Fig. 8). Heterogeneous areas of stiffness were more present in the personalized lung cartography of the heavy smokers (PY ≥ 20).

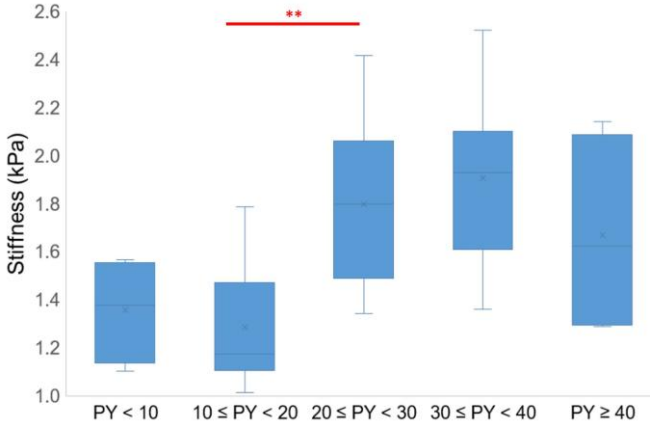

Fig. 8 Box-plots of the lung stiffness values for five groups of smokers according to different ranges of pack-year (PY). Symbol ** indicates statistical significance (p < 0.01) from two-sample Mann-Whitney's test.

The repeatability results obtained with the intra-class correlation coefficient (ICC) demonstrated excellent agreement between the two operators (ICC (95% limits-of-agreement): 0.93 (0.84 to 0.98)) for measuring MRE lung stiffness. In addition, an excellent ICC was also obtained for the repeatability of successive measurements (ICC (95 % limits-of-agreement): 0.92 [0.84 to 0.95]).

Of note, no statistically significant correlation was found between CT density and MRE-derived stiffness (r = 0.0979, p = 0.5817).

IV. Discussion

The World Health Organization (WHO) Framework Convention on Tobacco Control (WHO FCTC) is deeply involved in several actions to control the tobacco epidemic [42]. Their approach is to discourage individuals from starting smoking [43] and to encourage those who already smoke to quit the habit. Messages are relayed by awareness campaigns in the media, on cigarette packaging, and by health professionals. In the present study, we propose another type of awareness using a comprehensible report composed of visual color cartography, reflecting the general condition of smokers' lungs.

The originality of this work is that it personalizes the mechanical result using the patient's own lung density, a density that varies from one person to another. The validity of the lung density value was demonstrated with a phantom using two imaging modalities (CT, MR). It is worth noting that analysis of CT lung density is rare, and the measurements will be made by the radiologist if nodules or tumors are present in the lungs. However, the significant increase in CT density for the heavy smokers (PY $\geq$ 20) demonstrated the value of evaluating CT density even though no lung anomalies have been visually identified by the radiologist. Heavy smokers (PY $\geq$ 20) had denser CT lung tissue and the present result was in harmony with the study by Karimi et al. [44] who also found a relationship between high resolution CT density and the level of inflammation in smokers. It is well known that nicotine can induce lung inflammation and chronic obstructive pulmonary disease (COPD), and these pathological outcomes showed modification in the extracellular matrix (ECM) [45], [46]. A smoker's lung tissue may become denser due to the changes occurring in ECM stiffness (rigidity of the proteins, collagen vs elastin ratio) [47] which plays an important role in the biomechanical properties impacting the lungs' behavior [48]. However, the broad distribution of density data for each smoker group indicates that for a same level of consumption the lungs' response is patient-specific. It is noticed that 1) the PY subgrouping (Fig. 5) for the lung density do not show an evident increase in function of the consumption and 2) the density for PY $\leq$ 10 is visually relatively high (Fig. 5). It will be necessary to increase the number of smokers per PY group to strengthen the conclusion.

In radiology, MRI tests are almost never performed on the lungs due to them being mainly composed of air, leading to poor resolution. Thus, as expected, a non-significant difference in density was found between both smoker groups, and even though heterogeneous color distribution of density values was observed inside the different MR cartographies, the comparison of MR mappings in relation to PY was not possible. This result was mainly due to the difference of pixel size and slice thickness between CT and MR modalities. Indeed, CT acquisition provided a better spatial resolution (CT_pixel size: 0.72 mm vs MR_pixel size: 3.75 mm). In addition, for the same lung volume of interest, data were collected on 96 slices with CT vs only 4 slices with MR due to the thinner slice (CT_thickness: 0.625 mm vs MR_thickness: 15 mm). However, acquiring personalized MR density is a key step in the post processing for generating the personalized cartography of stiffness. For this reason, the present study focused on carefully validating the MR density data with another imaging modality (i.e. CT) as well as with *in vitro* acquisition performed on an abdominal phantom.

In the literature, some studies have published a cartography of lung stiffness but comparing the data is difficult due to 1) the different imaging modalities (ultrasound, CT, elastography, etc.), 2) the region of investigation, such as the pleural surface with ultrasound, 3) the different parameters (frequency, …). Most of the MRE lung studies were realized on healthy volunteers [30], [31], and rare studies [32], [35], have performed MRE lung tests on ILD (interstitial lung disease) (N=15) and CF (cystic fibrosis) (N = 3) patients, respectively. Similar MRE protocols, at the same frequency, were performed to assess the stiffness of healthy (about 1 kPa) [49] and pathological [30] lungs and an increase in stiffness in fibrotic tissue was demonstrated. The similar range of data between the stiffness of both smoker groups and other MRE lung studies demonstrates the MRE technique's ability to characterize the lungs of smokers. In addition, the cartography of stiffness revealed heterogeneous spatial distribution of values indicating lung areas which were more or less affected. The stiffer areas were mainly present in lungs with a pack-year of more than 20, leading to functional changes, which may explain the respiratory discomfort felt by the smoker patients. This PY number is considered as a high risk for lung cancer [6]. Interestingly, MRE stiffness cartography highlighted abnormal mechanical properties in lung areas, while CT acquisition showed a grey level of normal tissue. In addition, the higher stiffness found for the heavy smokers was associated with higher CT density, demonstrating the sensitivity of the MRE technique to the physiological (such as the extracellular matrix) changes in the lungs and could potentially predict lung pathogenesis caused by smoking. In addition, the present results show that the stiffness parameter is more sensitive ($p < 0.001$) than CT density ($p < 0.05$) and is measured without radiation, which is important for the follow-up of lung disease.

The present study had several limitations, such as not using the pulmonary function test (PFT), and it would be interesting to simultaneously analyze the PFT and stiffness results. Also, the way of obtaining PY per patient might bias the results if the patients were not accurate enough in their PY estimation. In addition, the MRE lung protocol could be improved by bilateral comparisons of lung data, decreasing breath hold time, etc. In complement, a numerical work could be associated with the development of a constitutive law integrating several parameters such as age, gender, physical activity, pack-years, etc. to predict the mechanical behavior of smokers' lungs. In perspective, MRE data could be integrated into finite element modeling to validate a parametric poromechanical lung model [50].

V. Conclusion

MRE could provide 1) a personalized cartography of stiffness revealing how smoking changes the chemical and cellular structure of the smoker's lung, 2) a regular uptake of the lung's mechanical behavior in smokers and 3) a potential

prevention of future disease resulting in both economic and social impacts. In addition, MRE could help tobacco specialists better understand how the lungs recover once someone stops smoking.

ACKNOWLEDGMENT

We wish to thank Dr Ehman at Mayo Clinic, Rochester, Minnesota, USA for MRE support.

REFERENCES

[1] World Health Organization, « WHO report on the global tobacco epidemic, 2023: protect people from tobacco smoke ». Consulted on: 11 november 2024. [On line]. Available at: https://www.who.int/publications/i/item/9789240077164

[2] J. V. Aredo *et al.*, « Tobacco Smoking and Risk of Second Primary Lung Cancer », *Journal of Thoracic Oncology*, vol. 16, nº 6, Art. nº 6, june 2021, doi: 10.1016/j.jtho.2021.02.024.

[3] R. Beaglehole et R. Bonita, « Harnessing tobacco harm reduction », *The Lancet*, vol. 403, nº 10426, Art. nº 10426, feb. 2024, doi: 10.1016/S0140-6736(24)00140-5.

[4] T. Gredner *et al.*, « Impact of tobacco control policies implementation on future lung cancer incidence in Europe: An international, population-based modeling study », *The Lancet Regional Health – Europe*, vol. 4, may 2021, doi: 10.1016/j.lanepe.2021.100074.

[5] C. L. Paul *et al.*, « The social context of smoking: A qualitative study comparing smokers of high versus low socioeconomic position », *BMC Public Health*, vol. 10, nº 1, Art. nº 1, apr. 2010, doi: 10.1186/1471-2458-10-211.

[6] P. F. Pinsky et B. S. Kramer, « Lung Cancer Risk and Demographic Characteristics of Current 20–29 Pack-Year Smokers: Implications for Screening », *JNCI: Journal of the National Cancer Institute*, vol. 107, nº 11, Art. nº 11, nov. 2015, doi: 10.1093/jnci/djv226.

[7] M. C. Willemsen, U. Mons, et E. Fernández, « Tobacco control in Europe: progress and key challenges », *Tobacco Control*, vol. 31, nº 2, Art. nº 2, mars 2022, doi: 10.1136/tobaccocontrol-2021-056857.

[8] J. Hartmann-Boyce *et al.*, « Electronic cigarettes for smoking cessation », *Cochrane Database of Systematic Reviews*, nº 11, Art. nº 11, 2022, doi: 10.1002/14651858.CD010216.pub7.

[9] R. Beaglehole *et al.*, « Nicotine without smoke: fighting the tobacco epidemic with harm reduction », *The Lancet*, vol. 394, nº 10200, Art. nº 10200, august 2019, doi: 10.1016/S0140-6736(19)31884-7.

[10] N. A. Nitta *et al.*, « Exposure to the heated tobacco product IQOS generates apoptosis-mediated pulmonary emphysema in murine lungs », *American Journal of Physiology-Lung Cellular and Molecular Physiology*, vol. 322, nº 5, Art. nº 5, may 2022, doi: 10.1152/ajplung.00215.2021.

[11] R. Talhout *et al.*, « Hazardous Compounds in Tobacco Smoke », *International Journal of Environmental Research and Public Health*, vol. 8, nº 2, Art. nº 2, févr. 2011, doi: 10.3390/ijerph8020613.

[12] World Health Organization, « WHO global report on trends in prevalence of tobacco use 2000-2025, fourth edition ». Consulted on: 11 november 2024. [On line]. Available at: https://www.who.int/publications/i/item/9789240039322

[13] W. W. Labaki *et al.*, « Causes of and Clinical Features Associated with Death in Tobacco Cigarette Users by Lung Function Impairment », *Am J Respir Crit Care Med*, vol. 208, nº 4, Art. nº 4, august 2023, doi: 10.1164/rccm.202210-1887OC.

[14] GOLD, « Global Initiative for Chronic Obstructive Lung Disease », Global Initiative for Chronic Obstructive Lung Disease - GOLD. Consulted on: 11 november 2024. [On line]. Available at: https://goldcopd.org/

[15] A. Strzelak *et al.*, « Tobacco Smoke Induces and Alters Immune Responses in the Lung Triggering Inflammation, Allergy, Asthma and Other Lung Diseases: A Mechanistic Review », *International Journal of Environmental Research and Public Health*, vol. 15, nº 5, Art. nº 5, may 2018, doi: 10.3390/ijerph15051033.

[16] D. Douglas *et al.*, « Tobacco smoking is associated with combined pulmonary fibrosis and emphysema and worse outcomes in interstitial lung disease », *American Journal of Physiology-Lung Cellular and Molecular Physiology*, vol. 325, nº 2, Art. nº 2, august 2023, doi: 10.1152/ajplung.00083.2023.

[17] C. Sousa *et al.*, « Diffuse smoking-related lung diseases: insights from a radiologic-pathologic correlation », *Insights into Imaging*, vol. 10, nº 1, Art. nº 1, july 2019, doi: 10.1186/s13244-019-0765-z.

[18] A. W. K. Yeung, « The "As Low As Reasonably Achievable" (ALARA) principle: a brief historical overview and a bibliometric analysis of the most cited publications », *Radioprotection*, vol. 54, nº 2, Art. nº 2, april 2019, doi: 10.1051/radiopro/2019016.

[19] C. Brower et M. M. Rehani, « Radiation risk issues in recurrent imaging », *British Journal of Radiology*, vol. 94, nº 1126, Art. nº 1126, oct. 2021, doi: 10.1259/bjr.20210389.

[20] K. Hasse *et al.*, « Systematic feasibility analysis of performing elastography using reduced dose CT lung image pairs », *Medical Physics*, vol. 47, nº 8, Art. nº 8, 2020, doi: 10.1002/mp.14112.

[21] K. Hasse, J. Neylon, et A. P. Santhanam, « Feasibility and quantitative analysis of a biomechanical model-guided lung elastography for radiotherapy », *Biomed. Phys. Eng. Express*, vol. 3, nº 2, Art. nº 2, feb. 2017, doi: 10.1088/2057-1976/aa5d1c.

[22] M. K. Chakouch *et al.*, « How magnetic resonance elastography (MRE) could provide biomechanical properties to complete computed tomography (CT) scan lung diagnostic? », *Computer Methods in Biomechanics and Biomedical Engineering*, vol. 26, nº sup1, Art. nº sup1, august 2023, doi: 10.1080/10255842.2023.2246304.

[23] X. Zhang *et al.*, « An Ultrasound Surface Wave Technique for Assessing Skin and Lung Diseases », *Ultrasound in Medicine and Biology*, vol. 44, nº 2, Art. nº 2, feb. 2018, doi: 10.1016/j.ultrasmedbio.2017.10.010.

[24] B. Zhou *et al.*, « Ultrasound Elastography for Lung Disease Assessment », *IEEE Transactions on Ultrasonics, Ferroelectrics, and Frequency Control*, vol. 67, nº 11, Art. nº 11, nov. 2020, doi: 10.1109/TUFFC.2020.3026536.

[25] S. Huang *et al.*, « Evaluation of connective tissue disease-related interstitial lung disease using ultrasound elastography: a preliminary study », *Quantitative Imaging in Medicine and Surgery*, vol. 12, nº 7, Art. nº 7, july 2022, doi: 10.21037/qims-21-1205.

[26] Y. Chen *et al.*, « Two-dimensional shear wave elastography: a new tool for evaluating respiratory muscle stiffness in chronic obstructive pulmonary disease patients », *BMC Pulmonary Medicine*, vol. 22, nº 1, p. 441, nov. 2022, doi: 10.1186/s12890-022-02231-4.

[27] M. Chakouch *et al.*, « MR elastography of the human lung », *State of the Art in Bioengineering*, vol. 2, nº 1, Art. nº 1, févr. 2022, Consulté le: 7 july 2024. [En ligne]. Disponible sur: https://hal.science/hal-03562216

[28] G. E. Leclerc *et al.*, « Analysis of liver viscosity behavior as a function of multifrequency magnetic resonance elastography (MMRE) postprocessing », *Journal of Magnetic Resonance Imaging*, vol. 38, nº 2, Art. nº 2, 2013, doi: 10.1002/jmri.23986.

[29] S. F. Bensamoun *et al.*, « Monitoring of lung stiffness for long-COVID patients using magnetic resonance elastography (MRE) », *Magnetic Resonance Imaging*, vol. 115, p. 110269, jan. 2025, doi: 10.1016/j.mri.2024.110269.

[30] Y. K. Mariappan *et al.*, « MR elastography of human lung parenchyma: Technical development, theoretical modeling and in vivo validation », *Journal of Magnetic Resonance Imaging*, vol. 33, nº 6, Art. nº 6, 2011, doi: 10.1002/jmri.22550.

[31] F. Fakhouri *et al.* « Free-breathing MR elastography of the lungs: An in vivo study », *Magnetic Resonance in Medicine*, vol. 87, nº 1, p. 236-248, 2022, doi: 10.1002/mrm.28986.

[32] J. P. Marinelli *et al.*, « Quantitative assessment of lung stiffness in patients with interstitial lung disease using MR elastography », *Journal of Magnetic Resonance Imaging*, vol. 46, nº 2, Art. nº 2, 2017, doi: 10.1002/jmri.25579.

[33] U. Schneider, E. Pedroni, et A. Lomax, « The calibration of CT Hounsfield units for radiotherapy treatment planning », *Phys. Med. Biol.*, vol. 41, nº 1, Art. nº 1, jan. 1996, doi: 10.1088/0031-9155/41/1/009.

[34] S. Holverda *et al.*, « Measuring lung water: Ex vivo validation of multi-image gradient echo MRI », *Journal of Magnetic Resonance Imaging*, vol. 34, nº 1, Art. nº 1, 2011, doi: 10.1002/jmri.22600.

[35] Y. Cho *et al.*, « Magnetic Resonance Elastography and Computational Modeling Identify Heterogeneous Lung Biomechanical Properties during Cystic Fibrosis », *Research Square*, 2024. doi: 10.21203/rs.3.rs-4125891/v1.

[36] R. J. Theilmann *et al.*, « Quantitative MRI measurement of lung density must account for the change in T with lung inflation », *Journal of Magnetic Resonance Imaging*, vol. 30, nº 3, Art. nº 3, 2009, doi: 10.1002/jmri.21866.

[37] Y. K. Mariappan *et al.*, « Estimation of the absolute shear stiffness of human lung parenchyma using 1H spin echo, echo planar MR elastography », *Journal of Magnetic Resonance Imaging*, vol. 40, nº 5, p. 1230-1237, 2014, doi: 10.1002/jmri.24479.

[38] P. Pouletaut *et al.*, « Impact of Hepatic Iron Overload in the Evaluation of Steatosis and Fibrosis in Patients with Nonalcoholic Fatty Liver Disease Using Vibration-Controlled Transient Elastography (VCTE) and MR Imaging Techniques: A Clinical Study », *IRBM*, vol. 44, nº 3, Art. nº 3, june 2023, doi: 10.1016/j.irbm.2022.100750.

[39] A. M. Silva *et al.*, « Magnetic resonance elastography: evaluation of new inversion algorithm and quantitative analysis method », *Abdom Imaging*, vol. 40, nº 4, Art. nº 4, april 2015, doi: 10.1007/s00261-015-0372-5.

[40] R Core Team. R: A Language and Environment for Statistical Computing. Vienna, Austria: R Foundation for Statistical Computing, 2016. Accessed July 7, 2024. Available at: https://www.R-project.org/.

[41] J. L. Fleiss, B. Levin, et M. C. Paik, « The Measurement of Interrater Agreement », in *Statistical Methods for Rates and Proportions*, John Wiley & Sons, Ltd, 2003, p. 598-626. doi: 10.1002/0471445428.ch18.

[42] H. Ollila *et al.*, « Tobacco endgame goals and measures in Europe: current status and future directions », *Tobacco Control*, june 2024, doi: 10.1136/tc-2024-058606.

[43] N. B. Rajani, J. Goyal, et F. T. Filippidis, « First experience with nicotine products and transition to regular tobacco use: a secondary data analysis in 28 European countries », *BMJ Open*, vol. 14, nº 3, Art. nº 3, mars 2024, doi: 10.1136/bmjopen-2023-080818.

[44] R. Karimi *et al.*, « Lung density on high resolution computer tomography (HRCT) reflects degree of inflammation in smokers », *Respir Res*, vol. 15, nº 1, Art. nº 1, feb. 2014, doi: 10.1186/1465-9921-15-23.

[45] R. Annoni *et al.*, « Extracellular matrix composition in COPD », *European Respiratory Journal*, vol. 40, nº 6, Art. nº 6, dec. 2012, doi: 10.1183/09031936.00192611.

[46] A. J. Booth *et al.*, « Acellular Normal and Fibrotic Human Lung Matrices as a Culture System for In Vitro Investigation », *Am J Respir Crit Care Med*, vol. 186, nº 9, p. 866-876, nov. 2012, doi: 10.1164/rccm.201204-0754OC.

[47] E. S. White, « Lung Extracellular Matrix and Fibroblast Function », *Annals ATS*, vol. 12, nº Supplement 1, Art. nº Supplement 1, mars 2015, doi: 10.1513/AnnalsATS.201406-240MG.

[48] J. K. Burgess *et al.*, « The extracellular matrix – the under-recognized element in lung disease? », *The Journal of Pathology*, vol. 240, nº 4, Art. nº 4, 2016, doi: 10.1002/path.4808.

[49] M. K. Chakouch *et al.*, « Viscoelastic shear properties of in vivo thigh muscles measured by MR elastography », *Journal of Magnetic Resonance Imaging*, vol. 43, nº 6, Art. nº 6, 2016, doi: 10.1002/jmri.25105.

[50] C. Laville *et al.*, « Comparison of optimization parametrizations for regional lung compliance estimation using personalized pulmonary poromechanical modeling », *Biomech Model Mechanobiol*, vol. 22, nº 5, 1541-1554, oct. 2023, doi: 10.1007/s10237-023-01691-9.